arXiv:2111.10727v1 [math.AP] 12 Nov 2021

HIGH SPOTS FOR THE ICE-FISHING PROBLEM WITH SURFACE TENSION

NATHAN WILLIS, CHEE HAN TAN, CHRISTEL HOHENEGGER, AND BRAXTON OSTING

Abstract. In the ice-fishing problem, a half-space of fluid lies below an infinite rigid plate ("the ice") with a hole. In this paper, we investigate the ice-fishing problem including the effects of surface tension on the free surface. The dimensionless number that describes the effect of surface tension is called the Bond number. For holes that are infinite parallel strips or circular holes, we transform the problem to an equivalent eigenvalue integro-differential equation on an interval and expand in the appropriate basis (Legendre and radial polynomials, respectively). We use computational methods to demonstrate that the high spot, *i.e.,* the maximal elevation of the fundamental sloshing profile, for the IFP is in the interior of the free surface for large Bond numbers, but for sufficiently small Bond number the high spot is on the boundary of the free surface. While several papers have proven high spot results in the absence of surface tension as it depends on the shape of the container, as far as we are aware, this is the first study investigating the effects of surface tension on the location of the high spot.

1. Introduction

Sloshing refers to the motion of a liquid free surface, *i.e.,* the interface between the liquid in the container and the air above, inside partially filled containers [Ibr05; FT09]. Liquid sloshing is a ubiquitous phenomenon, ranging from the oscillation of fuel in road tank vehicles and liquid-propellant rockets to seiches in lakes and harbors induced by earthquakes to our everyday experience in carrying a cup of coffee. Liquid sloshing has detrimental impacts on the stability and structural safety of stationary or moving vessels. For example, violent fuel sloshing within spacecraft fuel tanks produces highly localized pressure on tank walls, leading to deviation from its planned flight path or compromising its structural integrity.

Surface tension, defined as a force per unit length, is the intermolecular force required to contract the liquid surface to its minimal surface area. Examples of surface tension effects include the nearly spherical shape of liquid droplets and the ability of small insects to walk on water. The dimensionless parameter measuring the relative magnitudes of gravitational and surface tension forces is referred to as the Bond number and given by $\mathrm{Bo} = \rho g \ell_c^2/\sigma$, where $\rho > 0$ is the constant fluid density, ℓ_c is a characteristic length scale of the container, and $\sigma > 0$ is the surface tension coefficient. For example, in a microgravity environment, the magnitude of body forces is tiny and surface tension forces predominate. Mathematically, surface tension is incorporated into the sloshing model via the Young-Laplace equation, $\Delta P = -2\sigma H$, which asserts that the pressure difference ΔP between the inside and the outside of the fluid free surface is proportional to the mean surface curvature H. Recently a variational characterization of fluid sloshing with surface tension was derived in [THO17] and an isoperimetric problem was considered in [THO21].

In this paper, we investigate the ice-fishing problem (IFP), including the effects of surface tension on the free surface. The IFP studies the problem of free oscillations of an incompressible, inviscid

Date: November 23, 2021.

2010 *Mathematics Subject Classification.* 76B10, 76B45, 65R15, 33C45, 45C05, 35P15, 47G20.

Key words and phrases. fluid sloshing, surface tension, high spots conjecture, generalized eigenvalue problem, orthogonal polynomials.

C.H. Tan and B. Osting acknowledge partial support from NSF DMS 17-52202.

fluid for an irrotational flow in a half space bounded above by an infinite rigid plane where the free surface is some aperture in the plane; see Figure 1. We consider the cases where the aperture is either a circular hole or an infinite parallel strip. We denote the equilibrium free surface by $\mathcal{F}$, the wetted boundary by $\mathcal{B}$, and the fluid domain by $\mathcal{D}$.

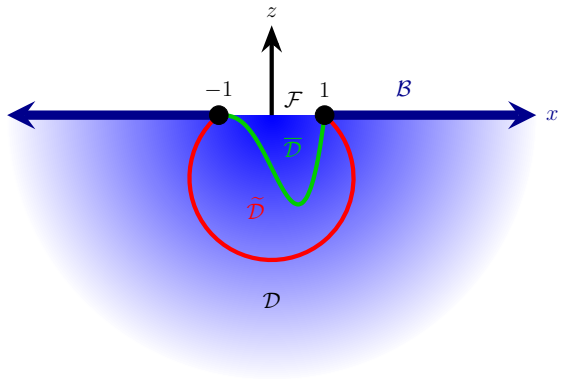

FIGURE 1. An illustration of the fluid domain $\mathcal{D}$ and boundary $\mathcal{B} \cup \mathcal{F} \cup \partial\mathcal{F}$ for a cross section of the infinite parallel strip. Multiple bounded domains are shown to demonstrate the domain monotonicity property of the fundamental sloshing frequency, *i.e.,* $\omega_1^2(\overline{\mathcal{D}}) \leq \omega_1^2(\widetilde{\mathcal{D}})$.

1.1. **Previous results.** In the absence of surface tension, Moiseev [Moi64] established the property of domain monotonicity for the square of the fundamental (smallest) sloshing frequency ω_1^2. Namely, for any two bounded containers $\overline{\mathcal{D}}, \widetilde{\mathcal{D}}$ with an identical $\mathcal{F}$ and $\overline{\mathcal{D}} \subset \widetilde{\mathcal{D}}$, we have that $\omega_1^2(\overline{\mathcal{D}}) \leq \omega_1^2(\widetilde{\mathcal{D}})$; see Figure 1. This result is an immediate consequence of the variational characterization of ω_1^2. It follows that the fundamental sloshing frequency for the IFP furnishes the universal upper bound for the fundamental sloshing frequency of arbitrary containers with coinciding $\mathcal{F}$. In the presence of surface tension, it was shown that this domain monotonicity result continues to hold for a free surface that is freely allowed to move at its boundary [THO17].

The IFP with zero surface tension has been well-studied in the past few decades. Davis [Dav70] reformulated the infinite parallel strip problem as an integral equation involving Green's function. He expressed the velocity potential as the infinite sum of Legendre polynomials and applied the principle of deformation of contours to give $\{\omega_j^2\}_{j=1}^{\infty}$ as the eigenvalues of an infinite symmetric matrix. Furthermore, he obtained approximations for ω_j^2 by computing the eigenvalues of the truncated matrix and derived a fourth-order asymptotic expansion for higher eigenvalues. Henrici, Troesch, and Wuytack [HTW70] formulated the IFP with a circular or strip-like aperture including a decay condition at infinity for the fluid velocity field and derived an equivalent Fredholm integral equation for the velocity potential in the aperture using potential theory. Miles [Mil72] recasts the IFP as formulated by Henrici et al. [HTW70] to a homogeneous Fredholm integral equation for the velocity distribution in the aperture. Troesch [Tro73] transformed the IFP onto a bounded domain using the Kelvin inversion. Fox and Kuttler [FK83] transformed the infinite parallel strip problem into an equivalent weighted problem on a semi-infinite strip employing a conformal map. Most authors computed upper bounds for ω_j^2 on their equivalent problems using the Rayleigh-Ritz method.

Of particular interest is the problem of determining the location of the high spots, *i.e.,* the maximal elevation of the sloshing profile ξ. *Unless otherwise noted, when discussing the high spots it is assumed that ξ is the fundamental sloshing profile.* The study of these high spots is motivated

as a fluid-analogue to the Hot Spots Conjecture: "For any second eigenfunction of the Neumann Laplacian, the extremal values of this eigenfunction are only attained on the boundary of the triangle" [Pol]. Indeed, [KK09, Proposition 3.1] proved that the hot spots problem and the high spots problem are equivalent for an upright cylindrical tank in the absence of surface tension. In two dimensions, the high spot is located on $\partial\mathcal{F}$ for any $\mathcal{B}$ that can be written as a negative C^2 function on $\mathcal{F}$ such that $\mathcal{B}$ is not tangent to $\mathcal{F}$ at their common endpoints [KK09]. This result extends to three dimensions when considering the previously described two-dimensional container as the cross section of a finite canal [KK11]. For a radially-symmetric, convex, bounded container such that $\mathcal{D}$ is contained in the upright cylinder $\mathcal{F}\times(-\infty,0)$, the high spot is located on $\partial\mathcal{F}$ [KK12]. Concerning the IFP, it is known that the high spot is located in the interior of $\mathcal{F}$ when $\mathcal{F}$ is either a circular hole or an infinite parallel strip [KK09]. All these results rely on the property that ξ is proportional to the trace of the fundamental sloshing mode Φ_1 on $\overline{\mathcal{F}}$ when the fluid oscillates freely with the fundamental sloshing frequency. Finally, it was conjectured that for a bounded planar domain with smooth $\mathcal{B}$ such that at least one angle between $\mathcal{B}$ and $\mathcal{F}$ is greater than $\pi/2$, the high spot is located in the interior of $\mathcal{F}$ [KK09].

1.2. **Main results.** In this paper, we investigate how the presence of surface tension affects the location of the high spot for IFP, focusing on an infinite parallel strip and a circular hole. We use computational tools to demonstrate that the high spot is in the interior of $\mathcal{F}$ for large Bo, but for sufficiently small Bo the high spot is on $\partial\mathcal{F}$. We plot the location of the high spot on the x-axis in the infinite parallel strip in Figure 2a and the circular hole in Figure 2b for varying Bo. The fundamental sloshing profiles for $\mathrm{Bo} = 1, 20, 100$ are shown in Figure 2c. In both cases, *we observe that as* Bo *increases, the high spot moves from the boundary of* $\mathcal{F}$ *to the interior of* $\mathcal{F}$. This transition happens at $\mathrm{Bo}^* = 8.98461$ for the infinite parallel strip and at $\mathrm{Bo}^* = 4.63462$ for the circular hole. The vertical asymptote corresponds to the high spot location for $\mathrm{Bo} \to \infty$, *i.e.,* in the absence of surface tension. To obtain these results we reduce the three-dimensional problem to a one-dimensional integro-differential equation. This one-dimensional problem is then solved approximately in orthogonal polynomial spaces, specifically Legendre polynomials for the infinite parallel strip and radial polynomials for the circular hole, resulting in a generalized eigenvalue problem for sloshing frequencies. For a circular hole, the critical value Bo^* is obtained by finding the value of Bo at which the concavity of the sloshing profile at the boundary switches from positive to negative. We show that this condition can be reformulated as a fixed point problem, yielding a precise value of Bo^*.

1.3. **Outline.** This paper is structured as follows. In Section 2, we describe the derivation of IFP with surface tension and an equivalent Fredholm integro-differential equation. In Sections 3 and 4, we describe the reduction of this equation when the aperture is an infinite parallel strip and a circular hole, respectively. In each section, we start by writing out the specific integro-differential equation, before deriving the associated weak form. The weak form is numerically solved in a Legendre polynomial space in Subsection 3.1 and in a radial polynomial space in Subsection 4.1, yielding a generalized eigenvalue problem. Examples of sloshing profiles and frequencies as well as convergence of the numerical schemes are presented in Subsections 3.2 and 4.2. In Section 5, we provide a justification for the location of the high spot for a radial hole that is based on determining the concavity at $r = 1$. This justification depends on the numerical results, but is intended to provide a basis for future analytical work on this point. We conclude in Section 6 with a discussion.

2. Model Derivation

The IFP can be described as the limiting case of the linear sloshing problem in a bounded domain with identical aperture; see [THO17, Appendix A] for a detailed derivation of the linear sloshing

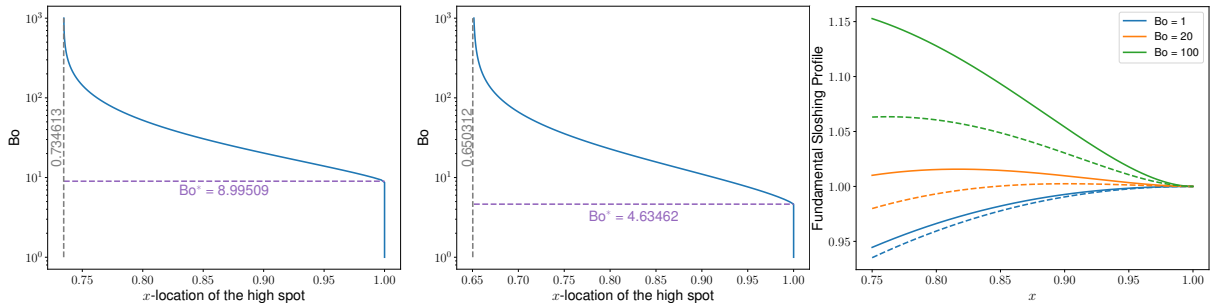

(a) Infinite parallel strip

(b) Circular hole

(c) Fundamental sloshing profile

FIGURE 2. Plot of the location of the high spot for (a) an infinite parallel strip and (b) a circular hole for varying Bo. The location of the high spot for the limiting case $\mathrm{Bo} \to \infty$ is marked with a vertical asymptote. (c) The fundamental sloshing profiles near the boundary $x = 1$ for both the infinite parallel strip (dashed lines) and the circular hole (solid lines) for $\mathrm{Bo} = 1, 20, 100$.

problem with surface tension on a bounded domain. We choose the halfwidth of the equilibrium free surface $\mathcal{F}$ as the characteristic length scale ℓ_c and nondimensionalize all lengths by ℓ_c, time by $t_c := \sqrt{\ell_c/g}$, and velocity by ℓ_c/t_c. Let $\mathbf{x} = (x, y, z)$ be dimensionless Cartesian coordinates such that the z-axis is directed vertically upward, perpendicular to the ice sheet. Let $\Phi(\mathbf{x})$ be the velocity potential with a time-harmonic factor $\cos(\omega t)$ removed and $\xi(x, y)$ be the sloshing profile, *i.e.,* the free surface displacement, with a time-harmonic factor $\sin(\omega t)$ removed, where ω is the natural sloshing frequency. Then, the IFP with Neumann boundary conditions is a dimensionless linear boundary spectral problem for (ω, Φ, ξ) defined by:

$$\Delta\Phi = 0 \quad \text{in} \quad \mathcal{D} = \left\{\mathbf{x} \in \mathbb{R}^3 \colon z < 0\right\}, \tag{1a}$$

$$\partial_z \Phi = 0 \quad \text{on} \quad \mathcal{B}, \tag{1b}$$

$$\partial_z \Phi = \omega\xi \quad \text{on} \quad \mathcal{F}, \tag{1c}$$

$$\xi - \frac{1}{\mathrm{Bo}}\Delta_{\mathcal{F}}\xi = \omega\Phi \quad \text{on} \quad \mathcal{F}, \tag{1d}$$

$$\partial_{\hat{\mathbf{n}}_{\mathcal{F}}}\xi = 0 \quad \text{on} \quad \partial\mathcal{F}, \tag{1e}$$

$$\int_{\mathcal{F}} \xi \, dA = 0. \tag{1f}$$

In the above equations, $\Delta_{\mathcal{F}}$ is the Laplacian operator on the free surface, and $\partial_{\hat{\mathbf{n}}_{\mathcal{F}}}$ is the derivative in the direction normal to the boundary of the free surface in the plane $z = 0$. The two cases we consider are

infinite parallel strip			circular hole		
$\mathcal{F}$	$=$	$\left\{\mathbf{x} \in \mathbb{R}^3 \colon \lvert x\rvert < 1, z = 0\right\}$	$\mathcal{F}$	$=$	$\left\{\mathbf{x} \in \mathbb{R}^3 \colon \lvert(x, y)\rvert < 1, z = 0\right\}$
$\mathcal{B}$	$=$	$\left\{\mathbf{x} \in \mathbb{R}^3 \colon \lvert x\rvert > 1, z = 0\right\}$	$\mathcal{B}$	$=$	$\left\{\mathbf{x} \in \mathbb{R}^3 \colon \lvert(x, y)\rvert > 1, z = 0\right\}$
$\partial\mathcal{F}$	$=$	$\left\{\mathbf{x} \in \mathbb{R}^3 \colon \lvert x\rvert = 1, z = 0\right\}$	$\partial\mathcal{F}$	$=$	$\left\{\mathbf{x} \in \mathbb{R}^3 \colon \lvert(x, y)\rvert = 1, z = 0\right\}$

The boundary condition Equation (1e) is necessary as surface tension introduces the linearized curvature term $\Delta_{\mathcal{F}}\xi$ into the model. It is known as the *contact line boundary condition* and it prescribes how the fluid free surface moves along the container wall. In this paper we consider the *free-end edge constraint* $\partial_{\hat{\mathbf{n}}_{\mathcal{F}}}\xi = 0$ on $\partial\mathcal{F}$.

Remark 2.1. For (ω, Φ, ξ) satisfying Equation (1), we have that Equation (1f) additionally gives no flow at infinity, *i.e.*, $|\nabla\Phi| \to 0$ as $|\mathbf{x}| \to \infty$. This result was shown in [HTW70] by expanding the kernel of the solution operator in spherical harmonics.

We solve Equation (1) by first expressing Φ as an integral operator acting on the Neumann boundary data $\omega\xi$, satisfying Equation (1a)-Equation (1c). We then plug this expression for Φ into Equation (1d) to derive an equivalent eigenvalue integro-differential equation for (ω, ξ). We start by considering the Laplace problem with compactly supported Neumann data

$$\Delta\Phi(\mathbf{x}) = 0 \quad \text{in} \quad \mathcal{D} = \left\{\mathbf{x} \in \mathbb{R}^3 \colon z < 0\right\}, \tag{2a}$$

$$\partial_z\Phi(\mathbf{x}) = f(\mathbf{x})\chi_{\mathcal{F}}(\mathbf{x}) \quad \text{on} \quad \partial\mathcal{D} = \left\{\mathbf{x} \in \mathbb{R}^3 \colon z = 0\right\}. \tag{2b}$$

Remark 2.2. By defining $f = \omega\xi$ it is easy to see that Equation (1e) is the compatibility condition, $\int_{\partial\mathcal{D}} f \, d\mathbf{x} = 0$, guaranteeing the existence and uniqueness, up to a constant, of the Neumann problem for Φ in the half-space.

Remark 2.3. If (ω, Φ, ξ) is a solution of Equation (1), then so are $(\omega, -\Phi, -\xi), (-\omega, -\Phi, \xi)$, and $(-\omega, \Phi, -\xi)$. There is no contradiction with the previous remark as for a given (ω, ξ) pair, Φ is unique up to a constant.

Definition 2.4. Let S be the operator, such that $\Phi(\mathbf{x})$ satisfying Equation (2) can be written as $\Phi(\mathbf{x}) = S[f\chi_{\mathcal{F}}](\mathbf{x}) + \Phi_\infty$, where Φ_∞ is constant and $Sf(\mathbf{x}) \to 0$ as $|\mathbf{x}| \to \infty$.

Examples of S for the infinite strip and circular holes are given in Sections 3 and 4, respectively. Comparing Equation (2b) and Equation (1b)-Equation (1c), we set $f = \omega\xi$, and plug in Equation (1d). This gives the following equation on the free surface,

$$\xi - \frac{1}{\mathrm{Bo}}\Delta_{\mathcal{F}}\xi = \omega^2\widehat{S}\xi + \omega\Phi_\infty. \tag{3}$$

Here $\widehat{S}$ is the restriction of S to the free surface $z = 0$. To remove Φ from this equation entirely, resulting in an eigenvalue integro-differential equation for (ω^2, ξ), we utilize Equation (1f). Motivated by [HTW70], we define the mean value operator to be $Mf = \frac{1}{|\mathcal{F}|}\int_{\mathcal{F}} f \, dA$ and next we consider $(I - M)$ where I is the identity operator. Note that $(I - M)$ applied to a constant yields 0 and $(I - M)\xi = \xi$. Therefore, applying $(I - M)$ to Equation (3) and including the appropriate conditions on ξ yields

$$\xi - \frac{1}{\mathrm{Bo}}(I - M)\Delta_{\mathcal{F}}\xi = \omega^2(I - M)\widehat{S}\xi \quad \text{on} \quad \mathcal{F}, \tag{4a}$$

$$\partial_{\hat{\mathbf{n}}_{\mathcal{F}}}\xi = 0 \quad \text{on} \quad \partial\mathcal{F}, \tag{4b}$$

together with $\int_{\mathcal{F}} \xi \, dA = 0$. The following theorem establishes equivalence between solutions of Equation (1) and Equation (4).

Theorem 2.5. *Let S be as in Definition 2.4 with $f = \omega\xi$. If (ω, ξ, Φ) is a solution to Equation (1) then (ω^2, ξ) solves Equation (4). Moreover, if (ω^2, ξ) is a solution to Equation (4) and we define $\Phi = \omega S\xi - \omega M\widehat{S}\xi - \frac{1}{\omega\mathrm{Bo}}M\Delta\xi$, then (ω, ξ, Φ) is a solution to Equation (1).*

Proof. The first statement is a direct result of the derivation of Equation (4) along with Remark 2.2. The second statement follows from the facts that $\omega M\widehat{S}\xi$ and $\frac{1}{\omega\mathrm{Bo}}M\Delta\xi$ are constant and therefore Equation (1a)-Equation (1c) are trivially satisfied due to the operator S. Restricting the definition of Φ to the free surface, we have $\Phi = \omega\,(I - M)\,\widehat{S}\xi - \frac{1}{\omega\mathrm{Bo}}M\Delta\xi$. Therefore, from Equation (4a) we find

$$\omega\Phi = \xi - \frac{1}{\mathrm{Bo}}(I - M)\Delta\xi - \frac{1}{\mathrm{Bo}}M\Delta\xi$$

such that (ω, ξ, Φ) satisfies Equation (1d). ■

3. Infinite parallel strip

In the case of the infinite parallel strip, we assume no dependence on y and therefore consider a cross section as in Figure 1. Using [HTW70; Wan14], we have the following representation of bounded solutions.

Lemma 3.1. *In the case of an infinite parallel strip with $\Phi(\mathbf{x}) = \Phi(x,z)$, there exists a bounded solution to Equation (2) of the form $\Phi(x,z) = S[f\chi_{[-1,1]}](x,z) + \Phi_\infty$, where*

$$S[f\chi_{[-1,1]}](x,z) = -\frac{1}{2\pi}\int_{-1}^{1} \ln\left((x-s)^2+z^2\right) f(s)\,ds, \quad \Phi_\infty = \lim_{|(x,z)|\to\infty} \Phi(x,z).$$

Proof. The existence up to a constant follows from the compatibility condition. Since $(Sf)(x,z) \to 0$ as $|(x,z)| \to \infty$ [Van14], the constant is $\Phi_\infty = \lim_{|(x,z)|\to\infty} \Phi(x,z)$. The facts that Φ satisfies Equation (2) and that Φ is bounded can be found in [Wan14]. ■

Lemma 3.1 gives the form of S as in Definition 2.4 with restriction to $z = 0$ given by $\widehat{S}\xi(x) = -\frac{1}{\pi}\int_{-1}^{1} \ln|x-s|\xi(s)\,ds$. Therefore, using Theorem 2.5, plugging into Equation (4) and keeping in mind that $\Phi(\mathbf{x}) = \Phi(x,z)$, we are seeking solutions of the following integro-differential equation

$$\xi - \frac{1}{\mathrm{Bo}}(I-M)\xi'' = \omega^2(I-M)\widehat{S}\xi = \lambda\widehat{S}\xi \quad \text{on } (-1,1), \tag{5a}$$

$$\xi'(\pm 1) = 0, \qquad \int_{-1}^{1} \xi\,dx = 0. \tag{5b}$$

We now turn our attention to seeking weak eigenpairs of Equation (5). Define the Hilbert space $V = \left\{\xi \in H^2(-1,1) \colon \xi'(\pm 1) = 0,\ \int_{-1}^{1}\xi\,dx = 0\right\}$.

Definition 3.2. We say that $(\omega,\xi) \in \mathbb{R}\times V$ is a weak sloshing eigenpair of Equation (5) if the following holds for all $g \in V$:

$$\int_{-1}^{1}\left(\xi g + \frac{1}{\mathrm{Bo}}\xi' g'\right)dx = -\frac{\omega^2}{\pi}\int_{-1}^{1}\int_{-1}^{1} \ln|x-s|\xi(s)g(x)\,dsdx. \tag{6}$$

Equation (6) is formally obtained by multiplying Equation (5a) by g, integrating from -1 to 1, using integration by parts with the prescribed boundary conditions, and simplifying with the facts that $M\xi''$ and $M\widehat{S}\xi$ are constant and $\int_{-1}^{1} g dx = 0$.

3.1. Polynomial Approximation.

We seek approximate solutions to Equation (6) in a finite-dimensional polynomial space. Let p_j denote the normalized Legendre polynomial of degree $j \geq 1$ on $[-1,1]$ with respect to the weight 1, *i.e.*, $\int_{-1}^{1} p_j p_k\,dx = \delta_{jk}$. Following [She94], we define the spaces $P^{(n)} = \operatorname{span}\{p_0(x), p_1(x), \ldots, p_n(x)\}$ and $W^{(n)} = \left\{v \in P^{(n)} \colon v'(\pm 1) = 0,\ \int_{-1}^{1} v\,dx = 0\right\}$. Suppose (ω,ξ) is a weak sloshing eigenpair of the IFP, as in Definition 3.2, and let $\xi^{(n)}$ be the orthogonal projection of ξ to $W^{(n)}$ with respect to the $L^2(-1,1)$ inner product. In general [Can+88, Equation 9.4.10] we have

$$\left\|\xi - \xi^{(n)}\right\|_{H^\ell(-1,1)} \leq Cn^{-1/2}n^{2\ell-m}\|\xi\|_{H^m(-1,1)}$$

for $\xi \in H^m(-1,1)$ with $1 \leq \ell \leq m$. In particular, since $\xi \in V \subset H^2(-1,1)$ we have the a-priori convergence result that $\xi^{(n)} \to \xi$ in $H^1(-1,1)$ as $n^{-1/2}$ as $n \to \infty$. Furthermore, the convergence will be faster if ξ is more regular and, in practice, we observe a higher rate of convergence; see Subsection 3.2.

For every $j = 1, 2, 3, \ldots$, define the polynomial $q_j = (p_j - \beta_j p_{j+2})/\alpha_j$. First, we choose $\beta_j = \dfrac{j(j+1)\sqrt{2j+1}}{(j+2)(j+3)\sqrt{2j+5}}$ to satisfy the Neumann boundary condition. Note that if Dirichlet boundary conditions were prescribed, one would simply define $\beta_j = \dfrac{\sqrt{2j+1}}{\sqrt{2j+5}}$, *i.e.,* all the boundary data is stored in the constants β_j. Next, we choose $\alpha_j = \sqrt{1+\beta_j^2}$ to normalize the q_j polynomials such that $\int_{-1}^{1} q_j^2\, dx = 1$.

Lemma 3.3. *The set of polynomials $\{q_j\}_{j=1}^{n-2}$ for $n = 3, 4, \ldots$ constitutes a basis for $W^{(n)}$.*

Proof. The statement follows from [She94; APQ03]. ■

Therefore, the discrete weak formulation of the IFP is to find $(\omega, \xi^{(n)}) \in \mathbb{R} \times W^{(n)}$ such that for all $g \in W^{(n)}$:

$$\int_{-1}^{1} \left(\xi^{(n)} g + \frac{1}{\mathrm{Bo}} \left(\xi^{(n)}\right)' g' \right) dx = -\frac{\omega^2}{\pi} \int_{-1}^{1}\int_{-1}^{1} \ln|x-s| \xi^{(n)}(s) g(x)\, ds dx. \tag{7}$$

Theorem 3.4. *If $(\omega, \xi^{(n)}) \in \mathbb{R} \times W^{(n)}$ solves the discrete IFP Equation (7), then $(\omega, \xi^{(n)})$ solves the generalized eigenvalue problem for $i = 1, 2, \ldots, n-2$*

$$\sum_{j=1}^{n-2} c_j \left(M_{ij} + \frac{1}{\mathrm{Bo}} K_{ij} \right) = \omega^2 \sum_{j=1}^{n-2} c_j L_{ij}. \tag{8}$$

Here $M_{ij} = \int_{-1}^{1} q_i(x) q_j(x)\, dx$ is the mass matrix, $K_{ij} = \int_{-1}^{1} q_i'(x) q_j'(x)\, dx$ is the stiffness matrix, and $L_{ij} = -\int_{-1}^{1}\int_{-1}^{1} \ln|x-s| q_i(x) q_j(s)\, ds dx$, which are given by

$$\begin{aligned}
M_{ij} &= \delta_{ij} - \frac{\beta_i}{\alpha_i \alpha_{i+2}} \delta_{i+2,j} - \frac{\beta_{i-2}}{\alpha_{i-2}\alpha_i} \delta_{i-2,j}, \\
K_{ij} &= \frac{\beta_j \sqrt{2j+5}}{\alpha_j^2 \sqrt{2j+1}} (2j+1)(2j+3) \delta_{ij}, \\
L_{ij} &= \frac{-\tilde{L}_{ij} + \beta_i \tilde{L}_{i+2,j} + \beta_j \tilde{L}_{i,j+2} - \beta_i \beta_j \tilde{L}_{i+2,j+2}}{\alpha_i \alpha_j}, \\
\tilde{L}_{ij} &= \begin{cases} \dfrac{4}{\pi} \dfrac{\sqrt{2i+1}\sqrt{2j+1}}{(i+j)(i+j+2)(1-(i-j)^2)} & \text{if } i+j \text{ is even,} \\ 0 & \text{otherwise.} \end{cases}
\end{aligned}$$

Proof. We write $\xi^{(n)} = \sum_{j=1}^{n-2} c_j q_j$ and choose $g = q_i$ in Equation (7). Expanding the q_i and q_j polynomials and using [Dav70] we find the expression for L_{ij}. To compute M_{ij} and K_{ij}, it suffices to consider the case where $i \le j$ since they are symmetric expressions. Using orthonormality of the Legendre polynomials, p_i, the expression for M_{ij} follows. To obtain K_{ij}, we integrate by parts and use the fact that $q_i'(\pm 1) = 0$ for $W^{(n)}$ to get

$$K_{ij} = -\frac{1}{\alpha_j} \left[\int_{-1}^{1} q_i'' p_j\, dx - \beta_m \int_{-1}^{1} q_i'' p_{j+2}\, dx \right].$$

Since q_i'' is at most degree i and the Legendre polynomial p_i is orthogonal to any polynomial of lower degree, we see that $K_{ij} = 0$ if $i < j$ and

$$K_{jj} = \frac{\beta_j}{\alpha_j^2} \int_{-1}^{1} p_{j+2}'' p_j\, dx = \frac{\beta_j \sqrt{2j+5}}{\alpha_j^2 \sqrt{2j+1}} (2j+1)(2j+3).$$

The final value for K_{jj} follows from the orthonormality of p_j the polynomials togehter with the well-known relationship,

$$p_j''(x) = \sqrt{2j+1} \sum_{\substack{k=0 \\ k+j \text{ even}}}^{j-2} \left(k + \frac{1}{2}\right) \Big(j(j+1) - k(k+1)\Big) \frac{p_k(x)}{\sqrt{2k+1}}.$$

■

3.2. **Numerical Results.** We now solve Equation (8), which is a generalized eigenvalue problem of the form

$$\left(\mathbf{M} + \frac{1}{\mathrm{Bo}}\mathbf{K}\right)\boldsymbol{\xi} = \lambda \mathbf{L}\boldsymbol{\xi}, \quad \lambda := \omega^2, \tag{9}$$

where $(\boldsymbol{\xi})_i = c_i$ and $\mathbf{M}$, $\mathbf{K}$, $\mathbf{L}$, are square matrices. The mass matrix $\mathbf{M}$ is pentadiagonal, the stiffness matrix $\mathbf{K}$ is diagonal, and the matrix $\mathbf{L}$ is dense, but exhibits a checkerboard pattern as $L_{ij} = 0$ if $i + j$ is odd. Specifically, the only nonzero diagonals for $\mathbf{M}$ are the main diagonal and the second sub and super diagonals. It follows from Theorem 2.5 that the eigenvalues λ_j of Equation (9) approximate the first n of the natural sloshing frequencies of IFP squared.

	$\mathrm{Bo} = 1$	$\mathrm{Bo} = 10$	$\mathrm{Bo} = 50$	$\mathrm{Bo} = \infty$
$j = 1$	7.0326	2.5238	2.1162	2.0061
$j = 2$	37.7871	6.9032	4.1530	3.4533
$j = 3$	119.0961	16.5480	7.4307	5.1253

TABLE 1. First three eigenvalues for the Infinite Parallel Strip IFP with $\mathrm{Bo} = \{1, 10, 50, \infty\}$.

The first three eigenvalues of Equation (9) for $\mathrm{Bo} = 1, 10, 50, \infty$ with $n = 200$ are shown in Table 1. To validate our solution to the infinite parallel strip IFP for $\mathrm{Bo} = \infty$ we compared the eigenvalues to those found in Fox et al. [FK83] and found that for all eigenvalues reported our results fit within the bounds provided. A table of all previous results [HTW70; Dav70; Mil72] is given in [FK83] and it is the case that Fox et al. provides the tightest bounds among the zero surface tension results. To get an understanding of the surface tension effects on the fundamental sloshing frequency we note that $\dfrac{\lambda_1(\mathrm{Bo} = 1)}{\lambda_1(\mathrm{Bo} = \infty)} = 3.506$. That is, when the force due to surface tension is comparable to the gravitational force the fundamental sloshing frequency is increased to more than 300% of the value when surface tension is negligible.

Figure 3a illustrates the convergence plots of the first two sloshing frequencies, *i.e.,* $j = 1, 2$, and their corresponding sloshing profiles in Figure 3b for $\mathrm{Bo} = \{0.1, 1, 10\}$. The true solution (λ_j^*, ξ_j^*) is the highly resolved ($n = 2000$) solution from our method. We observe high rates of convergence for finite Bo for both the sloshing frequencies and the sloshing profiles. We note that the observed rate of convergence for $\xi^{(n)} \to \xi$ is much higher than the a-proiri estimate as discussed above.

The first three sloshing profiles for $j = 1, 2, 3$ are shown in Figure 4 for $\mathrm{Bo} = 1$ in Figure 4a, $\mathrm{Bo} = 1000$ in Figure 4b and $\mathrm{Bo} = \infty$ corresponding to the no surface tension case in Figure 4c. The sloshing profiles for IFP appear to be unchanged for $\mathrm{Bo} < 10$. Most interesting is the behavior of the high spot of the fundamental sloshing profile for moderate Bo. This will be further discussed in Section 5, here we simply note that for small Bo the high spot is located on $\partial\mathcal{F}$ whereas for large Bo the high spot has moved to interior of $\mathcal{F}$. This phenomenon is further demonstrated for $\mathrm{Bo} \in [10^0, 10^3]$ in Figure 2a.

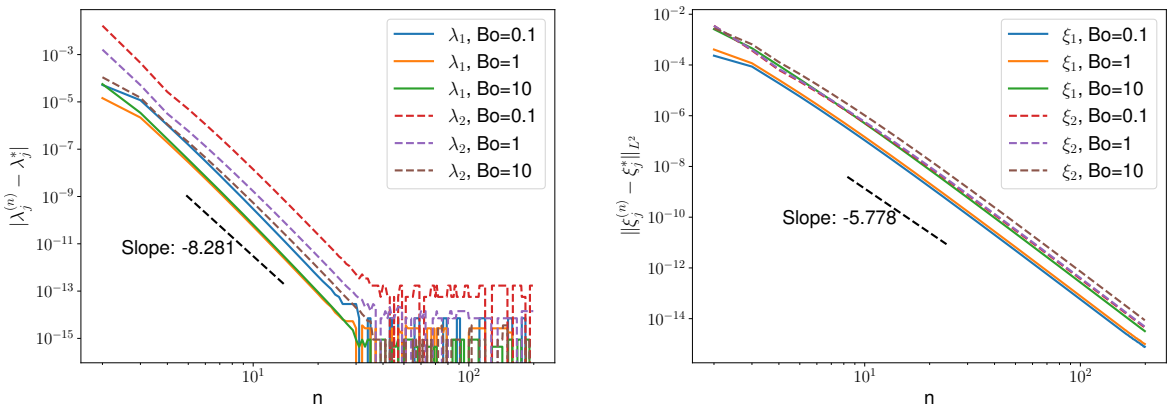

(a) λ_1, λ_2 convergence

(b) ξ_1, ξ_2 convergence

FIGURE 3. Log-log convergence plots of the first (solid) and second (dashed) eigenvalues and their corresponding sloshing profile for Bo $= 0.1, 1, 10$. The true solution is approximated with $n = 200$.

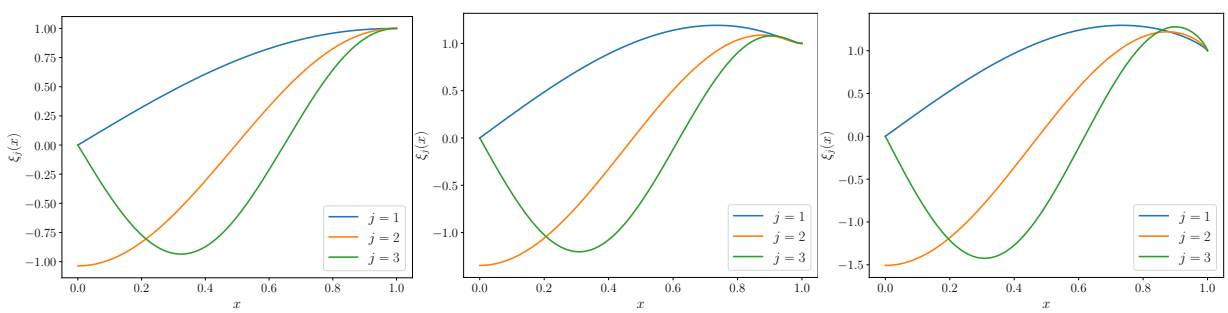

(a) Bo $= 1$

(b) Bo $= 1000$

(c) Bo $= \infty$

FIGURE 4. First three sloshing profiles for the infinite parallel strip for various Bo. Even though $\xi(x)$ is defined on $[-1, 1]$ solutions are only plotted on $[0, 1]$ since $\xi(x)$ is either even or odd.

4. CIRCULAR HOLE

For a circular hole, the outward normal to $\mathcal{F}$ in the plane $z = 0$ is in the radial direction. In this case, we transform the equations into cylindrical coordinates along the $z-$axis and we look for azimuthal solutions. To construct the integral operator S, we consider Equation (2) in cylindrical coordinates with $f(r, \theta) = f_m(r)\cos(m\theta)$ and $\mathcal{B}$ the unit disk. Therefore, we make the Ansatz $\Phi(r, \theta, z) = \Phi_m(r, z)\cos(m\theta)$ for $m \geq 0$ with the conditions that $\Phi_0(0, z)$ is bounded and that $\Phi_m(0, z) = 0$ for $m \geq 1$. Plugging the Ansatz into Equation (2) and canceling $\cos(m\theta)$ yields

$$\Delta_m \Phi_m + \partial_{zz}\Phi_m = 0 \quad \text{in} \quad \mathcal{D} = \left\{(r, z) \in \mathbb{R}^2 \colon r \geq 0 \; z < 0\right\}, \tag{10a}$$

$$\partial_z \Phi_m = f_m \chi_{[0,1)} \quad \text{on} \quad \partial\mathcal{D} = \{(r, z) \in \mathbb{R}^2 \colon r \geq 0 \; z = 0\}. \tag{10b}$$

In the above, $\Delta_m = \frac{1}{r}\partial_r(r\partial_r) - \frac{m^2}{r^2}$ is the Bessel differential operator. We remark that the compatibility condition is automatically satisfied for $m \geq 1$, whereas it becomes $\int_0^1 f_0 r dr = 0$ for $m = 0$. Furthermore, only for $m = 0$ can a new solution be obtained by adding a constant to any solution due to the term $\frac{m^2}{r^2}$ in Δ_m. We proceed to construct solutions to Equation (10) using the Hankel transform method. Following [Pie00], we define the Hankel transform pair, $F_m(k) = \mathcal{H}\{f\}(k)$, as

$$F_m(k) = \int_0^\infty r f(r) J_m(kr)\, dr \quad \text{and} \quad f(r) = \int_0^\infty k F_m(k) J_m(kr)\, dk$$

with J_m being the Bessel functions of the first kind. Using the fact that $\mathcal{H}\{\Delta_m f\}(k) = -k^2\mathcal{H}\{f\}(k)$ [Pie00], Equation (10a) becomes an integrable equation for $H_m = \mathcal{H}\{\Phi_m\}$. Looking for bounded solutions as $z \to -\infty$, the general solution has the form $H_m(k, z) = A(k)e^{kz}$. The constant of integration $A(k)$ is obtained using the Neumann boundary condition Equation (10b). Rearranging reveals that $kA(k) = \mathcal{H}\{f_m\}(k)$. We note that since $f_m(r)$ is compactly supported, the inverse Hankel transform is well defined [Pie00]. Therefore, we have a solution to the Neumann problem.

Lemma 4.1. *In the case of a radial hole with $f(r, \theta) = f_m(r)\cos(m\theta)$ where $f_m \in L^2_r(0, 1)$, there exists a bounded solution to Equation (2) that can be represented as*

$$\Phi(r, \theta, z) = \int_0^\infty \int_0^1 s f_m(s) J_m(ks) e^{kz} J_m(kr) ds dk \cos(m\theta) + c_m = Sf(r, \theta, z) + c_m$$

with $c_m = 0$ if $m \geq 1$. Furthermore, we have $Sf(r, \theta, z) \to 0$ as $(r, z) \to \infty$, θ fixed.

Proof. It is straightforward to show that Φ is a solution to Equation (10).

Let $G(k) = \int_0^1 \sqrt{s} f_m(s) \sqrt{s} J_m(ks)\, ds$. Using the Cauchy-Schwarz inequality and [Nis, p. 10.22.5], we find

$$|G(k)|^2 \leq \|f_m\|^2_{L^2_r(0,1)} \cdot \frac{1}{2}\Big[J_m^2(k) - J_{m-1}(k)J_{m+1}(k)\Big].$$

It follows that

$$\|G(k)\|^4_{L^4} \leq \|f_m\|^4_{L^2_r(0,1)} \int_0^\infty J_m^4(k) + J_{m-1}^2(k) J_{m+1}^2(k)\, dk < \infty,$$

since $J_m(k)$ is continuous on $[0, \infty)$ and $|J_m(k)| \leq k^{-1/3}$ for all k [Lan00]. Thus $G(k) \in L^4$. Next, using Hölder's inequality with $p = 4$ and $q = p/(p-1) = 4/3$, we obtain

$$|Sf| \leq \int_0^\infty |G(k) e^{kz} J_m(kr)|\, dk \leq \|G(k)\|_{L^4(0,\infty)} \left\| e^{kz} J_m(kr) \right\|_{L^{4/3}(0,\infty)}.$$

To estimate the second term on the right, we use the same bound as above on $|J_m(k)|$ and a change of variable. We have

$$\left\| e^{kz} J_m(kr) \right\|^{4/3}_{L^{4/3}(0,\infty)} \leq \int_0^\infty \frac{e^{4kz/3}}{(kr)^{4/9}}\, dk = \left(\frac{3}{4}\right)^{5/9} \frac{1}{(-z)^{5/9} r^{4/9}} \Gamma(5/9),$$

where $\Gamma(u)$ is the Gamma function. Since the last expression on the right goes to zero as $r^2 + z^2 \to \infty$ with $r > 0$ and $z < 0$, the claim follows. ■

Considering the form of the surface equation Equation (1d) for ξ in cylindrical coordinates and looking for azimuthal solutions, we make the same Ansatz $\xi(r, \theta) = \xi_m(r)\cos(m\theta)$. Therefore, for each $m \geq 0$, Lemma 4.1 gives the form of the integral operator S defined in Definition 2.4 with the restriction to $z = 0$ given by

$$\widehat{S}\xi(r, \theta) = \int_0^\infty \int_0^1 s \xi_m(s) J_m(ks) J_m(kr) ds dk \cos(m\theta).$$

Therefore, using Theorem 2.5, plugging into Equation (4a), transforming in cylindrical coordinates, using the Ansatz, noting that $M(\xi_m \cos(m\theta)) = 0$ for $m \geq 1$, and cancelling the cosine, we have the integro-differential equation

$$\xi_m - \frac{1}{\mathrm{Bo}}\Delta_m \xi_m = \omega^2 \widehat{S}_r \xi_m(r) \quad \text{for} \quad m \geq 1, \tag{11}$$

where $\widehat{S}_r \xi_m(r) = \int_0^\infty \int_0^1 \xi_m(r) s J_m(ks) J_m(kr) ds dk$ is the radial part of $\widehat{S}$. In the case $m = 0$, we recall that from Equation (1f), we require $\int_0^1 \xi_0 r\, dr = 0$. We have $\Phi = \Phi_0(r, z)$ and $\xi = \xi_0(r)$ so that application of Theorem 2.5 in cylindrical coordinates yields

$$\xi_0 - \frac{1}{\mathrm{Bo}}(I - M)\left(\frac{1}{r}(r\xi_0')'\right) = \omega^2 (I - M)\widehat{S}_r \xi_0(r) \quad \text{for} \quad m = 0. \tag{12}$$

The boundary conditions to Equation (11)-Equation (12) are $\xi_m'(1) = 0$, $\xi_0(0)$ bounded and $\xi_m(0) = 0$ for $m \geq 1$.

We now look for weak eigenpairs to Equation (11) and Equation (12). Define the Hilbert spaces

$$V_0 = \left\{ \xi_0 \in H_r^2(0,1) : \xi_0'(1) = 0, \xi_0(0) \text{ is bounded}, \int_0^1 r\xi_0\, dr = 0 \right\}$$
$$V_m = \left\{ \xi_m \in H_r^2(0,1) : \xi_m'(1) = 0, \xi_m(0) = 0 \right\}, \qquad m \geq 1,$$

where the subscript r indicates the weighted Sobolev space with respect to the weight function $w(r) = r$. Consider $m \geq 1$ and let g_m be a test function in V_m. Multiplying Equation (11) by $g(r)r$, integrating from 0 to 1, and using integration by parts along with the boundary conditions, we get the weak formulation

$$\int_0^1 \left(\xi_m g r + \frac{1}{\mathrm{Bo}} \frac{m^2}{r} \xi_m g + \frac{1}{\mathrm{Bo}} \xi_m' g' r \right) dr = \omega^2 \int_0^1 (\widehat{S}_r \xi_m)(r) g(r) r dr \quad \text{for } m \geq 1. \tag{13}$$

Let $m = 0$ and g_0 be a test function in V_0. Multiplying Equation (12) by $g(r)r$, integrating from 0 to 1, using integration by parts along with the boundary conditions, and remembering that the M operator produces a constant, we find the weak formulation

$$\int_0^1 \left(\xi_0 g r + \frac{1}{\mathrm{Bo}} \xi_m' g' r \right) dr = \omega^2 \int_0^1 (\widehat{S}_r \xi_0)(r) g(r) r dr. \tag{14}$$

It is obvious that Equation (13) and Equation (14) can be reformulated as a single weak formulation.

Definition 4.2. We say that $(\omega, \xi_m) \in \mathbb{R} \times V_m$ is a weak sloshing eigenpair of Equation (11), or Equation (12) when $m = 0$, if the following holds for all $g \in V_m$:

$$\int_0^1 \left(\xi_m g r + \frac{1}{\mathrm{Bo}} \frac{m^2}{r} \xi_m g + \frac{1}{\mathrm{Bo}} \xi_m' g' r \right) dr = \omega^2 \int_0^1 (\widehat{S}_r \xi_m)(r) g(r) r dr \quad \text{for } m \geq 0. \tag{15}$$

4.1. **Polynomial Approximation.** We look for approximate solutions to Equation (15) in a finite dimensional space. From the Hankel representation $\int_0^\infty k^2 A(k) J_m(kr) dk = f_m(r)$ with $f_m(r) = \omega \xi_m(r)$ along with the fact that $J_m(r) \sim \frac{r^m}{2^m \Gamma(m+1)}$ as $r \to 0$ [Nis, p. 10.7.3] we note that it is therefore necessary that $f_m(r) = O(r^m)$ as $r \to 0$. This fact motivates the use of the radial polynomials $h_j^m(r) = \mu_j^m r^m p_{j-1}^{(0,m)}(2r^2 - 1)$, with $p_j^{(\alpha,\beta)}(x)$ being the Jacobi polynomials and $\mu_j^m = 2\sqrt{j + \frac{1}{2}(m-1)}$. We note that these polynomials are orthogonal on $(0,1)$ with respect to the weight function r, *i.e.*, $\int_0^1 h_i^m(r) h_j^m(r) r dr = \delta_{ij}$. This fact follows simply from a change of variables, the orthogonality of Jacobi polynomials, and the fact that [Nis, p. 18.3.1] $\int_{-1}^1 (1+x)^m \left(p_{i-1}^{(0,m)}(x)\right)^2 dx = \frac{2^{m+1}}{2i+m-1}$. Moreover, we note that $\int_0^1 h_j^0 r\, dr = 0$ for $j = 2, 3, \ldots$. Now

we define $P_m^{(n)} = \text{span}\{h_0^m(x), h_1^m(x), \ldots, h_n^m(x)\}$ same as the infinite parallel strip and analogously define

$$W_m^{(n)} = \left\{ v \in P_m^{(n)} \colon v'(\pm 1) = 0 \text{ and } \int_0^1 vr\,dr = 0 \text{ if } m = 0 \right\}.$$

Lemma 4.3. *Suppose (ω, ξ_m) is a weak sloshing eigenpair of the circular hole IFP, as in Definition 4.2, and let $\xi_m^{(n)}$ be the orthogonal projection of ξ_m to $W_m^{(n)}$ with respect to the $L_r^2(0,1)$ inner product. When $m \geq 1$, if $\xi_m \in V_m \subset H_r^2(0,1)$ and $\frac{\xi_m}{r} \in L_r^2(0,1)$ then*

$$\left\| \xi_m - \xi_m^{(n)} \right\|_{L_r^2(0,1)} \leq C n^{-1} \left(m \left\| \frac{\xi_m(r)}{r} \right\|_{L_r^2(0,1)} + \left\| \xi_m'(r) \right\|_{L_r^2(0,1)} \right),$$

where the constant C is independent of n.

Remark 4.4. The result holds for $m = 0$ simply if $\xi_0 \in V_0$.

Proof. We denote the space of L^2 integrable functions on $(-1,1)$ with respect to the Jacobi weight function $w(x) = (1-x)^\alpha (1+x)^\beta$ as $L^2_{\alpha,\beta}$. Now, we note that $\sum_{j=1}^{n-2} \alpha_j h_j^m$ being the orthogonal projection of $\xi(r)$ with respect to the $L_r^2(0,1)$ inner product is equivalent to $\sum_{j=1}^{n-2} \frac{\alpha_j \mu_j^m}{2(2^{m/2})} P_{j-1}^{(0,m)}(x)$ being the orthogonal projection of $\frac{1}{2}\left(\frac{1}{x+1}\right)^{m/2} \xi\left(\sqrt{\frac{x+1}{2}}\right)$ with respect to the $L^2_{0,m}$ inner product. Then, by a change of variables and [GW04, Theorem 2.1] we have that

$$\begin{aligned}
\left\| \xi_m - \xi_m^{(n)} \right\|_{L_r^2(0,1)} &= \left\| \frac{1}{2}\left(\frac{1}{x+1}\right)^{m/2} \xi_m\left(\sqrt{\frac{x+1}{2}}\right) - \sum_{j=1}^{n-2} \frac{\alpha_j \mu_j^m}{2(2^{m/2})} p_{j-1}^{(0,m)}(x) \right\|_{L^2_{0,m}}, \\
&\leq C n^{-k} \left\| \frac{d^k}{dx^k} \left(\frac{1}{2}\left(\frac{1}{x+1}\right)^{m/2} \xi_m\left(\sqrt{\frac{x+1}{2}}\right) \right) \right\|_{L^2_{1,m+1}}.
\end{aligned}$$

To relate back to the $L_r^2(0,1)$ inner product we consider the specific case with $k = 1$, change variables, and use the triangle inequality to determine

$$\left\| \frac{d}{dx} \left(\frac{1}{2}\left(\frac{1}{x+1}\right)^{m/2} \xi\left(\sqrt{\frac{x+1}{2}}\right) \right) \right\|_{L^2_{1,m+1}} \leq m \left\| \frac{\xi_m(r)}{r} \right\|_{L_r^2(0,1)} + \left\| \xi_m'(r) \right\|_{L_r^2(0,1)},$$

and the result follows. ∎

To strongly enforce the boundary conditions we define $q_j^m = h_j^m + \beta_j h_{j+1}^m$, where the constant β_j is such that $(q_j^m)'(1) = 0$. We know [Nis, p. 18.6.1] that $P_n^{(0,m)} = \frac{(1)_n}{n!} = 1$ and that $\frac{d}{dr} P_{j-1}^{(0,m)}(1) = \frac{(j-1)(j+m)}{2}$, which comes from evaluating the Jacobi polynomial differential equation at 1, yielding $\left(h_j^m\right)'(1) = \mu_j^m m + 2\mu_j^m (j-1)(j+m)$. Therefore, we have that $\beta_j = -\frac{\mu_j^m (m + 2(j-1)(j+m))}{\mu_{j+1}^m (m + 2j(j+m+1))}$. Note that if Dirichlet boundary conditions were prescribed, one would simply define $\beta_j^m = -\frac{\mu_j^m}{\mu_{j+1}^m}$.

Therefore, the discrete weak formulation of Equation (15) is to find $(\omega, \xi_m^{(n)}) \in \mathbb{R} \times W^{(n)}$ such that for all $g \in W_m^{(n)}$:

$$\begin{aligned}
&\int_0^1 \left(\xi_m^{(n)}(r) g(r) + \frac{1}{\text{Bo}} \frac{m^2}{r} \xi_m^{(n)}(r) g(r) + \frac{1}{\text{Bo}} \left(\xi_m^{(n)}(r)\right)' g'(r) r \right) dr \\
&\quad = \omega^2 \int_0^1 \int_0^\infty \int_0^1 \xi_m^{(n)}(r) s J_m(ks) J_m(kr) g(r) r\,ds\,dk\,dr.
\end{aligned} \tag{16}$$

Theorem 4.5. *If $(\omega, \xi_m^{(n)}) \in \mathbb{R} \times W^{(n)}$ solves the radial discrete IFP Equation (16), then $(\omega, \xi^{(n)})$ solves the generalized eigenvalue problem for $i = 1, 2, \ldots, n$*

$$\sum_{j=1}^{n} a_j^m \left(M_{ij}^m + \frac{1}{\mathrm{Bo}} K_{ij}^m \right) = \omega^2 \sum_{j=1}^{n} a_j^m L_{ij}^m, \tag{17}$$

where $M_{ij}^m = \int_0^1 q_j^m q_i^m r\, dr$ is the mass matrix, $K_{ij}^m = \int_0^1 \left(\frac{m^2}{r} q_j^m q_i^m + (q_j^m)'(q_i^m)' r \right) dr$ is the stiffness matrix, and $L_{ij}^m = \int_0^1 \int_0^\infty \int_0^1 q_j^m(s) J_m(ks) s\, ds J_m(kr)\, dk q_i^m(r) r dr$. For the $m = 0$ case this simply needs to be edited to $\xi_m = \sum_{j=2}^{n} a_j^m q_j^m$ and it only holds for $i = 2, \ldots, n$. Moreover,

$$\begin{aligned}
M_{ij}^m &= \left(1 + \beta_i^2\right) \delta_{ij} + \beta_i \delta_{i+1,j} + \beta_{i-1} \delta_{i-1,j}, \\
K_{ij}^m &= -\mu_j^m \mu_{j+1}^m \left(\mu_j^{m+1}\right)^2 \beta_j^m \delta_{ij}, \\
L_{ij}^m &= \tilde{L}_{ij}^m + \beta_i \tilde{L}_{i+1,j}^m + \beta_j \tilde{L}_{i,j+1}^m + \beta_i \beta_j \tilde{L}_{i+1,j+1}^m, \\
\tilde{L}_{ij}^m &= \frac{\mu_j^m \mu_i^m}{4\pi \left((j+i+m-1)^2 - \frac{1}{4} \right) \left(\frac{1}{4} - (j-1)^2 \right)}.
\end{aligned}$$

Proof. Again, we write $\xi_m^{(n)} = \sum_{j=1}^{n} a_j^m q_j^m$ for $i = 1, 2, \ldots, n$ and we choose $g = q_i^m$ in Equation (15) to obtain the integral form of the matrices. The lengthy calculations to obtain the coefficients are given in Appendix A. ■

4.2. **Numerical Results.** Similar to the infinite parallel strip we are left to solve a generalized eigenvalue problem of the form Equation (9). In the circular hole problem, the mass matrix $\mathbf{M}$ is tridiagonal, the stiffness matrix $\mathbf{K}$ is diagonal, and the matrix $\mathbf{L}$ is dense. Again, it follows from Theorem 2.5 that the eigenvalues λ_j of Equation (9) approximate the first n of the natural sloshing frequencies of IFP squared.

The first three eigenvalues, for $m = 0, 1, 10$, of Equation (9) for the circular hole for $\mathrm{Bo} = 1, 10, 50, \infty$ with $n = 200$ are shown in Table 2. To validate our solution to the circular hole IFP for $\mathrm{Bo} = \infty$ we compared the eigenvalues to those found in Miles [Mil72] for $m = 0, 1, 2, 3$ and note that for all eigenvalues reported our results agree to the accuracy given by Miles (6 digits). Miles [Mil72] compares their results to that of Henrici et al. [HTW70] and finds their results to be as accurate or more accurate. Miles [Mil72] reports that results are given for $n = 16$. The current work presents results with $n = 64$ to recover the same, or better, accuracy. This is necessary due to the enforcement of boundary conditions in the current work, which is not present in the $\mathrm{Bo} = \infty$ problem and for this reason not considered in [Mil72]. In the circular hole problem, with $m = 1$ we have that $\dfrac{\lambda_1(\mathrm{Bo} = 1)}{\lambda_1(\mathrm{Bo} = \infty)} = 4.510$. That is, when the force due to surface tension is comparable to the gravitational force the fundamental sloshing frequency is increased to more than 400% of the value when surface tension is negligible.

Figure 5a illustrates the convergence plots of the sloshing frequencies $j = 1, 2$ with $m = 1$ and their corresponding sloshing profile in Figure 5b for $\mathrm{Bo} = \{0.1, 1, 10\}$. The true solution (λ_j^*, ξ_j^*) is the highly resolved ($n = 2000$) solution from our method. Convergence for the sloshing profiles is measured in the L^2-norm. In both the sloshing frequencies and sloshing profiles we observe a high rate of convergence. This rate of convergence is unaffected by the choice of m so only the results for $m = 1$ are shown.

The first three sloshing profiles, for $m = 0, 1, 2$, for $\mathrm{Bo} = \{1, 1000, \infty\}$ are shown in Figure 6. Again, the sloshing profiles for the circular hole appear to be unchanged for $\mathrm{Bo} < 10$. We observe

		Bo = 1	Bo = 10	Bo = 50	Bo = ∞
$m = 0$	$j = 1$	64.9935	10.2253	5.3528	4.1213
	$j = 2$	369.5505	43.5842	14.6085	7.3421
	$j = 3$	1100.4019	119.5281	32.3396	10.5171
$m = 1$	$j = 1$	12.4245	3.7758	2.9854	2.7548
	$j = 2$	172.4077	22.5719	9.2589	5.8921
	$j = 3$	665.6328	74.7182	22.1968	9.0329
$m = 10$	$j = 1$	1971.9593	209.8054	53.1458	13.5734
	$j = 2$	4740.2111	489.8354	112.0301	17.4838
	$j = 3$	8611.8754	880.1861	192.9290	21.0661

TABLE 2. Eigenvalues $j = 1, 2, 3$ for the azimuthal modes $m = 1, 2, 3$ and for Bo $= \{1, 5, 10, 20, 50, \infty\}$.

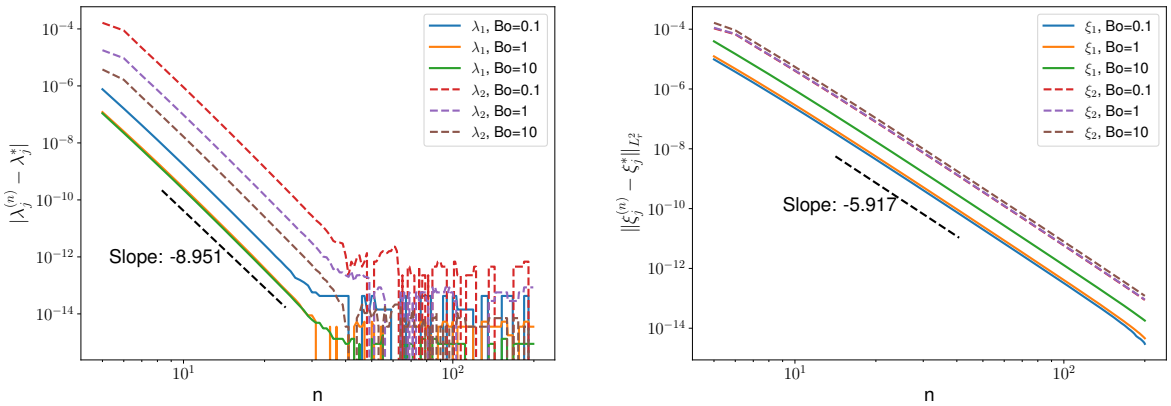

(a) λ_1, λ_2 convergence

(b) ξ_1, ξ_2 convergence

FIGURE 5. Log-log convergence plots of the first (solid) and second (dashed) eigenvalues and their sloshing profile for Bo $= 0.1, 1, 10$ with $m = 1$. The true solution is obtained with $n = 200$.

the same phenomenon as observed in the infinite parallel strip case that for small Bo the high spot is located on $\partial\mathcal{F}$ whereas for large Bo the high spot has moved to interior of $\mathcal{F}$. This can also be seen for Bo $\in [10^0, 10^3]$ in Figure 2b and it will be discussed further in Section 5.

5. High spot justification for a radial hole

In this section, we offer a justification for the main result that with sufficiently strong surface tension the high spot of the sloshing profile can be moved to the boundary of the free surface. We recall that previous results in the absence of surface tension, *i.e.,* Bo $\to \infty$, show that the high spot for a radial aperture is always inside the domain [KK09]. While we focus on the fundamental sloshing height, which corresponds to $m = 1$, $j = 1$, we demonstrate that the method described below to find the critical Bo such that the high spot is on the boundary applies for any $m \geq 1$ when such a Bo exists. Figure 2b plots Bo in terms of the location of the high spot for a radial hole, $m = 1$, and $j = 1$. It is obtained using Newton's method for $\xi_1'(r)$ and it shows that for

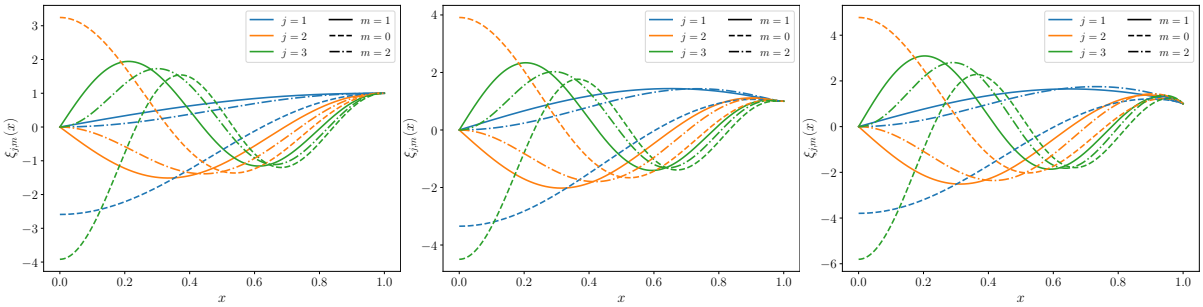

(a) Bo = 1 (b) Bo = 1000 (c) Bo = ∞

FIGURE 6. The first three sloshing profiles $j = \{1, 2, 3\}$ (blue, orange, green) for the IFP with a radial hole for $m = 0$ dashed, $m = 1$ solid and $m = 3$ dot dashed and for varying Bo.

$\mathrm{Bo} > \mathrm{Bo}^* = 4.63462$, the high spot is located in the interior and asymptotes to the known location $x = 0.650312$ for $\mathrm{Bo} \to \infty$ and that for $\mathrm{Bo} < \mathrm{Bo}^*$ the high spot is on the boundary.

To justify the numerical observation that for sufficiently small Bo the high spot is on the boundary, we remark that $r = 1$ is always a critical point of $\xi_m(r)$ in $[0, 1]$ as a consequence of the Neumann boundary condition. Furthermore, for $m \neq 0$, if $r = 1$ is a local minimum, then we must have by continuity of $\xi_m(r)$ that there exists at least one local maximum in $(0, 1)$ since $\xi_m(0) = 0$ and ξ_m is scaled such that $\xi_m(1) = 1$. Thus we start by finding the concavity of ξ_m at $r = 1$ and by determining $\mathrm{Bo} = \mathrm{Bo}^*$ for which $\xi_m''(1) = 0$, *i.e.,* where $\xi_m''(1)$ changes sign. To do so, we evaluate Equation (11) for $m \geq 1$ at $r = 1$ to get $\xi_m''(1) = m^2 + \mathrm{Bo}\left(1 - \omega^2 \widehat{S}_r \xi_m(1)\right)$. Here, we have used the fact that $\xi_m'(1) = 0$ and that $\xi_m(1) = 1$. Plugging in $\xi_m''(1) = 0$ and noting that (ω, ξ_m) depends on Bo we define

$$T(\mathrm{Bo}) = \frac{m^2}{\omega^2 \widehat{S}_r \xi_m(1) - 1},$$

and seek fixed points $\mathrm{Bo}^* = T(\mathrm{Bo}^*)$. The map $T(\mathrm{Bo})$ with $m = 1$ is plotted in Figure 7a in blue and the fixed points are the intersection with the black dashed line $y = \mathrm{Bo}$. Intuitively, to find the fixed points of $T(\mathrm{Bo})$ one would consider the iterative scheme $\mathrm{Bo}_{n+1} = T(\mathrm{Bo}_n)$. However, it is obvious from the slope at the fixed point in Figure 7a that these iterations will diverge. Additionally, we observe that $T(\mathrm{Bo})$ has a discontinuity where the denominator is zero. It follows naturally to instead consider the reciprocal map $1/T(1/x)$, where $x = 1/\mathrm{Bo}$, shown in Figure 7b for $m = 1$. This eliminates the observed discontuinity, but $x_{n+1} = 1/T(1/x_n)$ would still diverge away from the fixed point. Therefore, instead of iterating along a horizontal line from the map $1/T(1/x_n)$ to the line $x_{n+1} = x_n$ we iterate along a line passing through $(x_n, 1/T(1/x_n))$ with slope α to the line $x_{n+1} = x_n$, as illustrated by the red arrows in Figure 7b. We note that $\alpha = 0$ simply corresponds to a horizontal line which returns the classical cobweb scheme. Additionally, we see that if $\alpha = 1$ then the line we are iterating along is parallel to the line $x_{n+1} = x_n$ and the scheme is not sensible. With this idea, we define a new map

$$\widetilde{T}(x) = \frac{1}{1-\alpha}\left(\frac{1}{T\left(\frac{1}{x}\right)} - \alpha x\right), \tag{18}$$

shown in Figure 7c with $m = 1$, $\alpha = 3$, and now consider the iterative scheme $x_{n+1} = \widetilde{T}(x_n)$, as illustrated by the red arrows in Figure 7c. The following lemma follows by simple computations.

Lemma 5.1. *For $\alpha > 1$, Bo^* is a fixed point of T if and only if $x^* = \frac{1}{\mathrm{Bo}^*}$ is a fixed point of $\widetilde{T}$.*

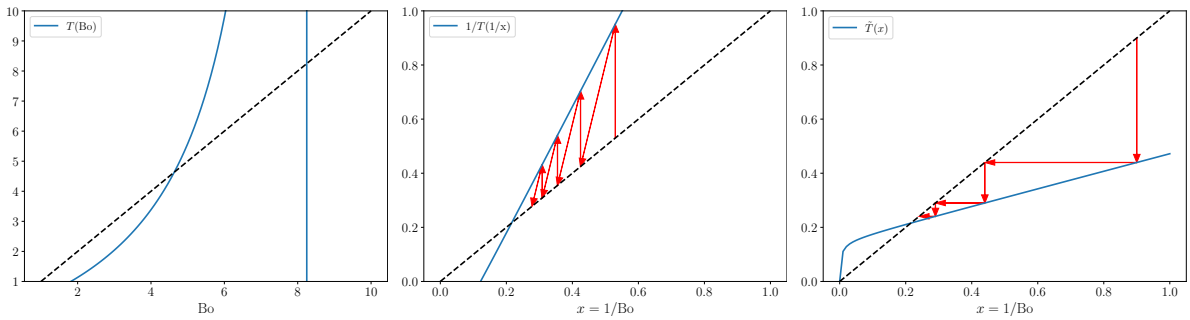

(a) $T(\mathrm{Bo})$ (b) $\frac{1}{T(\frac{1}{x})}$, $x = \frac{1}{\mathrm{Bo}}$ (c) $\widetilde{T}(x)$, $x = \frac{1}{\mathrm{Bo}}$

FIGURE 7. (a) $T(\mathrm{Bo})$ plotted for $\mathrm{Bo} \in [1, 10]$ and $m = 1$ where fixed points are at the intersection with the black dashed $y = \mathrm{Bo}$. We note the discontinuity of $T(\mathrm{Bo})$. (b) Reciprocal map $1/T(x)$ with $x = 1/\mathrm{Bo}$ together with the modified fixed point iteration with slope $\alpha = 3$ (c) New map $\widetilde{T}(x)$ with $x = 1/\mathrm{Bo}$ (blue) plotted for $x \in (0, 1]$, or $\mathrm{Bo} \in [1, \infty)$, $m = 1$, and $\alpha = 3$ where we note a fixed point for finite Bo at the intersection with the dashed line $y = x$ together with the fixed point iteration.

Algorithm 1 outlines the procedure to determine the value for Bo^*, the fixed point of $T(\mathrm{Bo})$, using the map $\widetilde{T}(x)$ and the equivalence of Lemma 5.1. To evaluate $\widehat{S}_r\xi_m(1)$, we use the polynomial approximation derived in Subsection 4.1 to write

$$\widehat{S}_r\xi_m(1) = \sum_{j=1}^{n} a_j^m \left((\widehat{S}_r h_j^m)(1) + \beta_j^m (\widehat{S}_r h_{j+1}^m)(1) \right), \tag{19}$$

where $\widehat{S}_r h_j^m(1) = \frac{\mu_j^m}{2\pi(j+m-\frac{1}{2})(j-\frac{1}{2})}$, see Appendix B for details.

Algorithm 1 Procedure to determine Bo^*

Require: $\mathrm{Bo} > 1$, $\alpha > 1$, $m \in \mathbb{N}$
  $x_0 \leftarrow 1/\mathrm{Bo}$
  while $|x_{n+1} - x_n| >$threshold **do**
    Solve Equation (9) for (ω, ξ_m) with $\mathrm{Bo} = 1/x_n$
    Evaluate $\omega^2(\widehat{S}_r\xi_m)(1)$ using Equation (19)
    $x_n \leftarrow \widetilde{T}(x_n)$
  end while
  return $1/x_n$

In Table 3, we report on the number of steps for Algorithm 1 to converge with a threshold of 10^{-14} for $\alpha = \{2, 3, 5, 10\}$ and $m = \{1, 2, 3, 4, 5\}$. As the number of steps were similar for all the n tested, we only give the results for $n = 20$. We note that the classical fixed point iteration corresponds to $\alpha = 0$ and the edited fixed point iteration should converge for any $\alpha > 1$, although it is expected that more iterations are necessary for convergence for larger α.

Values of Bo^* against the dimension of the solution space, $n = \{5, 20, 80\}$, and the radial mode, $m = \{1, 2, 3, 4, 5\}$ are given in Table 4. We note the agreement between the column $m = 1$ and the value given in Figure 2b.

	$m=1$	$m=2$	$m=3$	$m=4$	$m=5$
$\alpha=2$	29	40	92	195	540
$\alpha=3$	30	94	194	395	1066
$\alpha=5$	76	198	392	783	2088
$\alpha=10$	184	450	873	1726	4568

TABLE 3. Number of steps for Algorithm 1 to converge (with threshold $= 10^{-14}$) to a fixed point for $\alpha = 2, 3, 5, 10$, $m = 1, 2, 3, 4, 5$ and $n = 20$. All other values of n tested produced similar results.

	$m=1$	$m=2$	$m=3$	$m=4$	$m=5$
$n=5$	4.6342188	7.1574495	7.8108948	6.6284730	3.6110536
$n=20$	4.6346165	7.1588900	7.8137285	6.6328709	3.6171135
$n=80$	4.6346167	7.1588910	7.8137311	6.6328760	3.6171218

TABLE 4. Values of Bo^* for $n \in \{5, 20, 80\}$ and radial mode $m \in \{1, 2, 3, 4, 5\}$.

Theorem 5.2. *Consider the fundamental sloshing frequency $j = 1$. If $m \in \{1, \ldots, 5\}$, then Bo^* exists. Furthermore,*

(i) If $\mathrm{Bo} \in (\mathrm{Bo}^*, \infty)$, then the high spot is located in the interior.
(ii) If $\mathrm{Bo} \in [1, \mathrm{Bo}^*)$, then the high spot is on the boundary.

Proof. For $m \geq 6$, the equation $T(\mathrm{Bo}) = \mathrm{Bo}$ has no solution, so the high spot is inside the domain. We note that since $\xi_m(0) = 0$ and $\xi_m(r) \geq 0$, $r = 0$ is always a global minimum.

(i) Recall that $x = \frac{1}{\mathrm{Bo}}$. From Figure 7c, we observe that $\widetilde{T}(x) > x$ when $x < x^*$ so that $\widetilde{T}\left(\frac{1}{\mathrm{Bo}}\right) > \frac{1}{\mathrm{Bo}}$ whenever $\mathrm{Bo} > \mathrm{Bo}^*$. From the definition of $\widetilde{T}$ we have $\frac{1/T(\mathrm{Bo})-\alpha/\mathrm{Bo}}{1-\alpha} > \frac{1}{\mathrm{Bo}}$ and since $\alpha > 1$ this simplifies to $\frac{1}{T(\mathrm{Bo})} < \frac{1}{\mathrm{Bo}}$. Therefore, $\frac{\omega^2 \widehat{S}_r \xi_m(1)-1}{m^2} < \frac{1}{\mathrm{Bo}}$ so that $\xi_m''(1) = m^2 + \mathrm{Bo}(1 - \omega^2 \left(\widehat{S}_r \xi_m)(1)\right) > 0$. Thus $\xi_m''(1) > 0$ and along with the Neumann boundary conditions this implies that $\xi_m(1)$ is a local minimum and the high spot is in the interior.

(ii) Using similar calculations as above, we establish that $\xi_m''(1) < 0$. Since $\xi_m'(1) = 0$, we have that a local maximum occurs at $r = 1$. To conclude that $r = 1$ is a global maximum of $\xi_m(r)$, we see by inspection that there are no other critical points in $(0, 1)$. Thus, the high spot is on the boundary. ∎

Remark 5.3. When $\mathrm{Bo} \to \infty$, Theorem 5.2 implies that the high spot is in the interior for the problem without surface tension. This is consistent with previous results on the 2D IFP [KK09, Proposition 2.7] as well the 3D axially symmetric IFP [KK09, Theorem 3.2] where the authors neglect surface tension.

For further illustration, Section 5 shows the location of the first two nonzero roots of $\xi_1(r)$ for all Bo, one them always being $r = 1$. The derivative is expressed analytically as $\xi_1'(r) = \sum_{j=1}^{n} a_j^1 \frac{d}{dr} q_j^1(r)$ where the radial polynomial derivative uses derivatives of Jacobi polynomials and a simple root solver is used to find the zeros. Section 5 shows the expected horizontal asymptote $y = 0.650312$, the expected horizontal line $r = 1$ and the expected critical Bo^* where both curves intersect. For $\mathrm{Bo} < \mathrm{Bo}^*$, since the blue curve is always above the orange line, see Figure 8b for a blow up plot, we conclude that there are no critical points in $(0, 1)$.

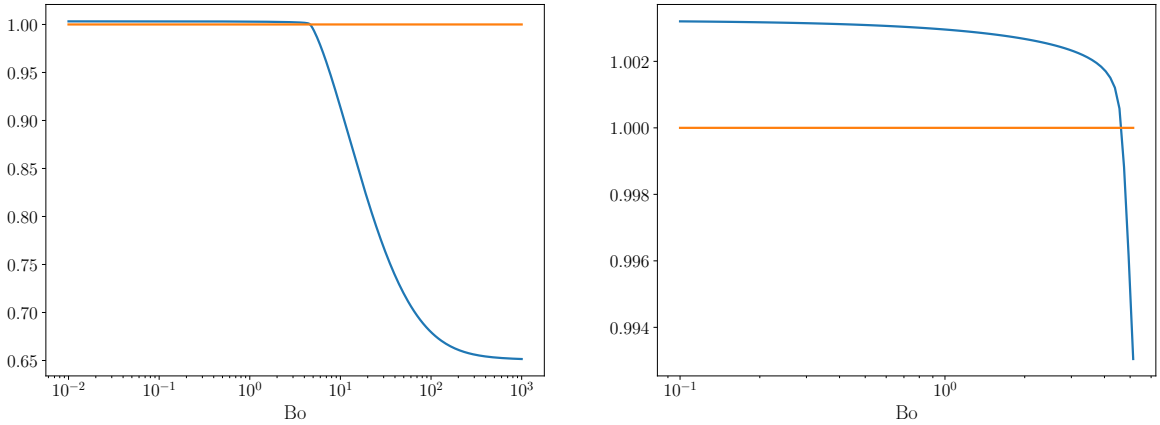

(a) Bo $\in [0.01, 1000]$

(b) Blow up for Bo $\in [0.1, 5]$

FIGURE 8. Location of the first two zeros of $\xi_m'(r)$ as a function of Bo. Because of the Neumann boundary condition, $r = 1$ is always a zero and corresponds to the orange line. The blue curve is obtained by numerically finding the first zero of $\xi_m'(r)$.

6. Discussion

This paper provides the first study on the ice fishing problem (IFP) including surface tension effects. Although the geometries considered are infinite parallel strips and circular holes, for any Bo, the results give an upper bound for the fundamental sloshing frequency for any container with the same free surface [THO17]. Building on previous studies without surface tension [Dav70; HTW70], we derived an integro-differential equation and proved the spectrum is equivalent to the spectrum of Equation (1). The novelty of this approach is that, for the considered geometries, the problem is transformed from an unbounded domain to a bounded one-dimensional domain. We numerically solved it by expanding in a polynomial basis, suitably chosen to satisfy the boundary conditions. We derived a closed form expression for the eigenvalue problem, which is a generalized eigenvalue matrix equation, and numerically approximated it.

We have assumed the free-end edge constraint, *i.e.,* the contact line slips freely along the vertical wall (edge of the ice hole) while intersecting it orthogonally. However, experimental evidence [CFF93; Dus79] reveals that the dynamic behavior of the contact line depends crucially on the contact angle, *i.e.,* the angle where the free surface meets a solid surface. It would be interesting to consider either the pinned-end edge constraint [BS79] or a dynamic contact line boundary conditions such as Hocking's linear wetting boundary condition [Hoc87a; Hoc87b], Dussan's nonlinear contact line model incorporating static contact angle hysteresis [Dus79], or a combination of Hocking's and Dussan's model that was recently proposed by Viola et al. [VBG18; VG18].

The eigenvalues from IFP are upper bounds for the corresponding eigenvalues for all other containers with coinciding free surface. It would therefore be of interest to know if the approximate eigenvalues presented here are perhaps upper or lower bounds for the true eigenvalues of IFP. In the absence of surface tension this was indeed considered in [FK83; HTW70]. The methods for the upper bounds were summarized in Section 1. For the lower bounds, Henrici et al. [HTW70] utilize the domain monotonicity property along with an infinitely deep cylinder or trough to bound the eigenvalues from below. When appropriate, they improve the bound by implementing the Krylov-Bogoliubov inequality on the integral operator to provide a tighter lower bound. Fox et al. [FK83] use the method of intermediate problems on an equivalent weighted problem on a

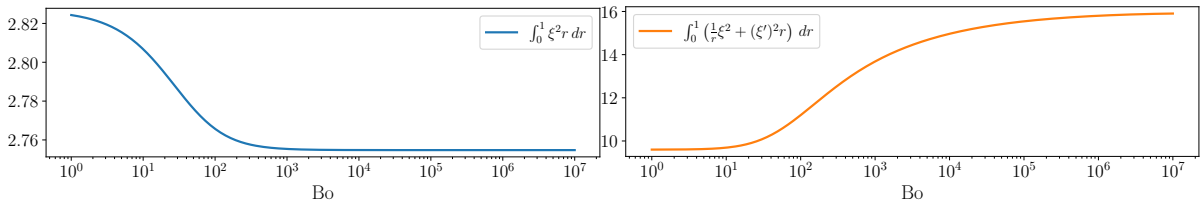

(a) $\int_0^1 \xi^2 r\, dr$ for Bo $\in [10^0, 10^7]$

(b) $\int_0^1 \left(\frac{1}{r}\xi^2 + (\xi')^2 r\right)\, dr$ for Bo $\in [10^0, 10^7]$

FIGURE 9. Comparison of the different contributions to the free surface energy to illustrate how the fundamental solution minimizes one versus the other depending on Bo with $m = 1$.

region where solutions are known. Taking advantage of known eigenvectors of the unweighted sloshing problem on the simple region, Fox et al. [FK83] produce much tighter lower bounds than otherwise observed while using low-dimensional matrices. While the domain monotonicity property holds when including surface tension, the other properties mentioned do not necessarily extend to the model considered here. Nonetheless, numerically bounding eigenvalues would be a significant advantage to this study and could be investigated in future work.

We numerically study how the location of the high spot depends on Bo. Using a simple fixed-point iteration we determine the value of Bo such that for any lower Bo the high spot is on the boundary of the free surface. This result compliments previous work [KK09] which shows that the high spot is always on the interior for the IFP in the absence of surface tension. For physical intuition, we recall the fundamental sloshing profile for the circular hole IFP minimizes the free surface energy,

$$\frac{\int_0^1 \xi_m^2 r\, dr + \frac{1}{\mathrm{Bo}} \int_0^1 \left(\frac{m^2}{r}\xi_m^2 + (\xi_m')^2 r\right)\, dr}{\int_0^1 (\widehat{S}_r \xi_m)(r)\xi_m(r) r dr}.$$

For simplicity, we scale the solution such that $\int_0^1 (\widehat{S}_r \xi_m)(r)\xi_m(r) r dr = 1$. For large Bo we are primarily minimizing $\int_0^1 \xi_m^2 r\, dr$, whereas for small Bo we are primarily minimizing $\int_0^1 \left(\frac{1}{r}\xi_m^2 + (\xi_m')^2 r\right)\, dr$. These different contributions to the free surface energy are shown in Figure 9. Therefore, we pay a more significant penalty for variation in the derivative when Bo is small and the intuition is that sloshing profiles with no interior extrema suffer less from this penalty. Motivated by this observation, we conjecture that *for any shape domain, given sufficiently small* Bo*, the high spot is located on the boundary of the free surface.*

ACKNOWLEDGMENTS

We would like to thank Akil Narayan and Fernando Guevara Vasquez for helpful conversations.

Appendix A. Matrix Elements Computations

The coefficients M_{ij}^m follow immediately from the orthogonality of the h_j^m polynomials and computation for $\tilde{L}_{ij}^m$ can be found in [Mil72]. Therefore, here we focus on showing that the stiffness matrix is diagonal and finding the values for those coefficients.

We first define $\tilde{K}_{ij}^m = \int_0^1 \left(\frac{m^2}{r} h_i^m h_j^m + (h_i^m)'(h_j^m)' r\right) dr$ so that we have $K_{ij}^m = \tilde{K}_{ij}^m + \beta_i \tilde{K}_{i+1,j}^m + \beta_j \tilde{K}_{i,j+1}^m + \beta_i \beta_j \tilde{K}_{i+1,j+1}^m$. Now we compute the $\tilde{K}_{ij}^m$ elements and start by recalling that $h_j^m = \mu_j^m r^m P_{j-1}^{(0,m)}(2r^2-1)$. From [Nis, p. 18.9.15] we have that

$$(h_j^m)' = \frac{m}{r} h_j^m + 2\mu_j^m r^{m+1}(m+j) P_{j-2}^{(1,m+1)}(2r^2-1),$$

and substituting this along with the definition of h_j^m into $\tilde{K}_{ij}$ we obtain

$$\tilde{K}_{ij}^m = 2\mu_j^m \mu_i^m \left(m^2 A_{ij}^m + \frac{m}{\mu_j^m}(i+m) B_{ij}^m + \frac{m}{\mu_i^m}(j+m) B_{ji}^m + (j+m)(i+m) C_{ij}^m \right),$$

where

$$\begin{aligned} A_{ij}^m &= \int_0^1 r^{m-1} P_{j-1}^{(0,m)}(2r^2-1) r^{m-1} P_{i-1}^{(0,m)}(2r^2-1) r\, dr, \\ B_{ij}^m &= \int_0^1 h_j^m r^m P_{i-2}^{(1,m+1)}(2r^2-1)\, dr, \\ C_{ij}^m &= 2\int_0^1 r^{m+1} P_{j-2}^{(1,m+1)}(2r^2-1) r^{m+1} P_{i-2}^{(1,m+1)}(2r^2-1)\, dr. \end{aligned}$$

To simplify A_{ij}^m we relate the $P_{j-1}^{(0,m)}$ Jacobi polynomials to the $P_{j-1}^{(0,m-1)}$ Jacobi polynomials in order to use the orthogonality of the h_j^{m-1} polynomials. First use the symmetry relation [Nis, Table 18.6.1] and then the connection sum formula [Nis, p. 18.18.14], with $\gamma = m$, $\alpha = m-1$, and $\beta = 0$, to get

$$P_{j-1}^{(0,m)}(x) = (-1)^j \frac{(j-1)!}{(m+1)_{j-1}} \sum_{\ell=1}^{j} \frac{m+2(\ell-1)}{m} \frac{(m)_{\ell-1}}{(\ell-1)!} (-1)^\ell P_{\ell-1}^{(0,m-1)}(x).$$

Since $m + 2(\ell-1) = \frac{1}{2}(\mu_\ell^{m-1})^2$ we have

$$r^{m-1} P_{j-1}^{(0,m)}(2r^2-1) = \frac{(-1)^j}{m} \frac{(j-1)!}{(m+1)_{j-1}} \sum_{\ell=1}^{j} \frac{\mu_\ell^{m-1}}{2} \frac{(m)_{\ell-1}}{(\ell-1)!} (-1)^\ell h_\ell^{m-1}. \tag{20}$$

Let $\kappa_{ij}^m = (-1)^{i+j} \frac{(j-1)!(i-1)!}{(m+1)_{j-1}(m+1)_{i-1}}$ and $\nu = \min(i,j)$, then we have

$$A_{ij}^m = \frac{\kappa_{ij}^m}{m^2} \sum_{\ell=1}^{j} \sum_{k=1}^{i} \frac{\mu_\ell^{m-1}\mu_k^{m-1}}{4\kappa_{\ell k}^{m-1}} \delta_{\ell k} = \frac{\kappa_{ij}^m}{m^2} \sum_{\ell=0}^{\nu-1} (m+2\ell) \left(\frac{(m)_\ell}{\ell!}\right)^2 = \frac{\kappa_{ij}^m}{m} \left(\frac{(m+1)_{\nu-1}}{(\nu-1)!}\right)^2.$$

The last simplification follows from $\left(\frac{(\nu-1)!}{(m+1)_{\nu-1}}\right)^2 \sum_{\ell=0}^{\nu-1} (m+2\ell) \left(\frac{(m)_\ell}{\ell!}\right)^2 = m$, which can be easily proved by induction om ν. Therefore,

$$A_{ij}^m = \frac{(-1)^{i+j}}{2m} \frac{(\min(i,j))_m}{(\max(i,j))_m}.$$

Next, we turn to B_{ij}^m and start by again using the connection sum formula [Nis, p. 18.18.14], this time with $\gamma = 1$, $\alpha = 0$, and $\beta = m$, to note that

$$r^m P_{i-1}^{(1,m)}(2r^2-1) = \frac{1}{2(m+i)} \sum_{\ell=1}^{i} \mu_\ell^m h_\ell^m(x). \tag{21}$$

Therefore, using the contiguous relation [Nis, p. 18.9.3] for $P_{i-2}^{(1,m+1)}$ along with the above relation for $r^m P_{i-1}^{(1,m)}$ and Equation (20) for $r^m P_{j-1}^{(0,m+1)}$ we have

$$r^m P_{i-2}^{(1,m+1)}(2r^2-1) = \frac{1}{2} \sum_{\ell=1}^{i} \frac{1}{m+i} \left(1 - (-1)^{i+\ell} \frac{(\ell)_m}{(i)_m}\right) \mu_\ell^m h_\ell^m(r).$$

From the orthogonality of h_j^m we now have

$$B_{ij}^m = \begin{cases} \dfrac{\mu_j^m}{2(m+i)} \left(1 - (-1)^{i+j} \dfrac{(j)_m}{(i)_m}\right) & j < i, \\ 0 & j \geq i. \end{cases}$$

Lastly, we turn to C_{ij}^m and use Equation (21) for $r^{m+1} P_{j-2}^{(1,m+1)}$ so that we can again use the orthogonality of the h_j^m polynomials. After simplifying we get

$$C_{ij}^m = \frac{\min(i,j)-1}{\max(i,j)+m} \tag{22}$$

With these expressions for A_{ij}^m, B_{ij}^m, and C_{ij}^m we now have that

$$\tilde{K}_{ij}^m = \mu_j^m \mu_i^m \left(m + 2(\min(i,j)-1)(\min(i,j)+m)\right).$$

Let us write the stiffness matrix as $K_{ij}^m = \Omega_{ij}^m + \beta_i \Omega_{i+1,j}^m$ with $\Omega_{ij}^m = \tilde{K}_{ij}^m + \beta_j \tilde{K}_{i,j+1}^m$. Due to the symmetry of K we assume without loss of generality that $j < i$ such that

$$\tilde{K}_{ij}^m = \mu_j^m \mu_i^m \left(m + 2(j-1)(j+m)\right).$$

Then, from the definition of β_j we have that $\Omega_{ij}^m = 0$ and $\Omega_{i,j+1}^m = 0$ if $j \neq i$. In the case that $i = j$ it follows from direct calculation that $K_{jj}^m = -\mu_j^m \mu_{j+1}^m \left(\mu_j^{m+1}\right)^2 \beta_j$.

Appendix B. Integral operator evaluated at $r = 1$

We start with the Hankel transform of h_j^m, given in [Mil72], to determine that

$$\widehat{S} h_j^m(1) = (-1)^{j-1} \mu_j^m \int_0^\infty \frac{J_{2j+m-1}(k) J_m(k)}{k}\, dk.$$

Using the Weber-Schafheitlin formula [Nis, p. 10.22.57], with $\alpha = 1 = \gamma$, $\mu = 2j+m-1$, and $\nu = m$, we have

$$\begin{aligned} \int_0^\infty \frac{J_{2j+m-1}(k) J_m(k)}{k}\, dk &= \frac{\Gamma\left(j+m-\frac{1}{2}\right)}{2\Gamma\left(\frac{3}{2}-j\right)\Gamma\left(j+\frac{1}{2}\right)\Gamma\left(j+m+\frac{1}{2}\right)}, \\ &= \frac{(-1)^j}{2\pi\left(j+m-\frac{1}{2}\right)\left(j-\frac{1}{2}\right)}, \end{aligned}$$

where we have simplified in a similar fashion as done in [Mil72]. It follows that

$$\widehat{S} h_j^m(1) = \frac{\mu_j^m}{2\pi\left(j+m-\frac{1}{2}\right)\left(\frac{1}{2}-j\right)}.$$

References

[APQ03] F. Auteri, N. Parolini, and L Quartapelle. "Essential imposition of Neumann condition in Galerkin–Legendre elliptic solvers". *J. Comput. Phys.* 185.2 (2003), pp. 427–444. DOI: 10.1016/S0021-9991(02)00064-5.

[BS79] T. B. Benjamin and J. C. Scott. "Gravity-capillary waves with edge constraints". *J. Fluid Mech.* 92.2 (1979), pp. 241–267. DOI: 10.1017/S0022112079000616.

[Can+88] C. Canuto et al. *Spectral Methods in Fluid Dynamics*. Springer, 1988. DOI: 10.1007/978-3-642-84108-8.

[CFF93] B. Cocciaro, S. Faetti, and C. Festa. "Experimental investigation of capillarity effects on surface gravity waves: non-wetting boundary conditions". *J. Fluid Mech.* 246 (1993), pp. 43–66. DOI: 10.1017/S0022112093000035.

[Dav70] A. Davis. "Waves in the presence of an infinite dock with gap". *IMA J. Appl. Math* 6.2 (1970), pp. 141–156. DOI: 10.1093/imamat/6.2.141.

[Dus79] E. Dussan. "On the spreading of liquids on solid surfaces: static and dynamic contact lines". *Annu. Rev. Fluid Mech.* 11.1 (1979), pp. 371–400. DOI: 10.1146/annurev.fl.11.010179.002103.

[FT09] O. M. Faltinsen and A. N. Timokha. *Sloshing*. Vol. 577. Cambridge University Press, 2009.

[FK83] D. W. Fox and J. R. Kuttler. "Sloshing frequencies". *Z. Angew. Math. Phys. ZAMP* 34.5 (1983), pp. 668–696. DOI: 10.1007/BF00948809.

[GW04] B.-y. Guo and L.-l. Wang. "Jacobi approximations in non-uniformly Jacobi-weighted Sobolev spaces". *J. Approx. Theory* 128.1 (2004), pp. 1–41. DOI: 10.1016/j.jat.2004.03.008.

[HTW70] P. Henrici, B. A. Troesch, and L. Wuytack. "Sloshing frequencies for a half-space with circular or strip-like aperture". *Z. Angew. Math. Phys. ZAMP* 21.3 (1970), pp. 285–318. DOI: 10.1007/BF01627938.

[Hoc87a] L. Hocking. "The damping of capillary–gravity waves at a rigid boundary". *J. Fluid Mech.* 179 (1987), pp. 253–266. DOI: 10.1017/S0022112087001514.

[Hoc87b] L. Hocking. "Waves produced by a vertically oscillating plate". *J. Fluid Mech.* 179 (1987), pp. 267–281. DOI: 10.1017/S0022112087001526.

[Ibr05] R. A. Ibrahim. *Liquid Sloshing Dynamics: Theory and Applications*. Cambridge University Press, 2005. DOI: 10.1017/CBO9780511536656.

[KK11] T Kulczycki and N Kuznetsov. "On the 'high spots' of fundamental sloshing modes in a trough". *Proceedings of the Royal Society A: Mathematical, Physical and Engineering Sciences* 467.2129 (2011), pp. 1491–1502. DOI: 10.1098/rspa.2010.0258.

[KK09] T. Kulczycki and N. Kuznetsov. "'High spots' theorems for sloshing problems". *Bull. Lond. Math. Soc.* 41.3 (2009), pp. 494–505. DOI: 10.1112/blms/bdp021.

[KK12] T. Kulczycki and M. Kwaśnicki. "On high spots of the fundamental sloshing eigenfunctions in axially symmetric domains". *Proc. Lond. Math. Soc.* 105.5 (2012), pp. 921–952. DOI: 10.1112/plms/pds015.

[Lan00] L. Landau. "Bessel functions: monotonicity and bounds". *Journal of the London Mathematical Society* 61.1 (2000), pp. 197–215.

[Mil72] J. W. Miles. "On the eigenvalue problem for fluid sloshing in a half-space". *Z. Angew. Math. Phys. ZAMP* 23.6 (1972), pp. 861–869. DOI: 10.1007/BF01596214.

[Moi64] N. N. Moiseev. "Introduction to the theory of oscillations of liquid-containing bodies". *Adv. Appl. Mech.* 8 (1964), pp. 233–289. DOI: 10.1016/S0065-2156(08)70356-9.

[Nis] *NIST Digital Library of Mathematical Functions*. http://dlmf.nist.gov/, Release 1.1.0 of 2020-12-15. F. W. J. Olver, A. B. Olde Daalhuis, D. W. Lozier, B. I. Schneider, R. F. Boisvert, C. W. Clark, B. R. Miller, B. V. Saunders, H. S. Cohl, and M. A. McClain, eds.

[Pie00] R. Piessens. "The Transforms and Applications Handbook". In: 3rd ed. Boca Raton: CRC Press, 2000. Chap. 9. DOI: 10.1201/9781315218915.

[Pol] *Polymath7: Establishing the hot spots conjecture for acute-angled triangles*. https://asone.ai/polymath/index.php?title=The_hot_spots_conjecture.

[She94] J. Shen. "Efficient spectral-Galerkin method I. Direct solvers of second-and fourth-order equations using Legendre polynomials". *SIAM J. Sci. Comput.* 15.6 (1994), pp. 1489–1505. DOI: 10.1137/0916006.

[THO17] C. H. Tan, C. Hohenegger, and B. Osting. "A variational characterization of fluid sloshing with surface tension". *SIAM J. Appl. Math.* 77.3 (2017), pp. 995–1019. DOI: 10.1137/16M1104330.

[THO21] C. H. Tan, C. Hohenegger, and B. Osting. *An Isoperimetric Sloshing Problem in a Shallow Container with Surface Tension.* preprint. 2021.

[Tro73] B. Troesch. "Sloshing frequencies in a half-space by Kelvin inversion". *Pacific J. Math.* 47.2 (1973), pp. 539–552. DOI: 10.2140/pjm.1973.47.539.

[Van14] J. Vannekoski. "The method of layer potentials: Unique solvability of the Dirichlet problem for Laplace's equation in C^1-domains with L^p-boundary data". PhD thesis. University of Helsinki, Helsinki, Finland, 2014.

[VBG18] F. Viola, P.-T. Brun, and F. Gallaire. "Capillary hysteresis in sloshing dynamics: a weakly nonlinear analysis". *J. Fluid Mech.* 837 (2018), pp. 788–818. DOI: 10.1017/jfm.2017.860.

[VG18] F. Viola and F. Gallaire. "Theoretical framework to analyze the combined effect of surface tension and viscosity on the damping rate of sloshing waves". *Physical Review Fluids* 3.9 (2018), p. 094801. DOI: 10.1103/PhysRevFluids.3.094801.

[Wan14] K. Wang. "On the Neumann problem for harmonic functions in the upper half plane". *J. Math. Anal. Appl.* 419.2 (2014), pp. 839–848. DOI: 10.1016/j.jmaa.2014.04.076.

Department of Mathematics, University of Utah, Salt Lake City, UT
Email address: willis@math.utah.edu

Department of Mathematics, Bucknell University, Lewisburg, PA
Email address: cht007@bucknell.edu

Department of Mathematics, University of Utah, Salt Lake City, UT
Email address: choheneg@math.utah.edu

Department of Mathematics, University of Utah, Salt Lake City, UT
Email address: osting@math.utah.edu